Examining the tolerance of GNSS receiver phase tracking loop under the effects of severe ionospheric scintillation conditions based on its bandwidth

Igor Ponte Portella (ORCID: 0000-0003-3464-3015)
Instituto de Pesquisas e Ensaios em Voo - IPEV
São José dos Campos, SP, Brazil
portellaipp@fab.mil.br

Alison de O. Moraes (ORCID: 0000-0002-6493-1694)
Instituto de Aeronáutica e Espaço - IAE
São José dos Campos, SP, Brazil
aom@ita.br

Marcelo da Silva Pinho (ORCID: 0000-0002-9393-8473)
Instituto Tecnológico de Aeronáutica - ITA
São José dos Campos, SP, Brazil
mpinho@ieee.org

Jonas de Sousasantos (ORCID: 0000-0001-6572-8009)
Instituto Tecnológico de Aeronáutica - ITA
São José dos Campos, SP, Brazil
jonasjss@ita.br

Fabiano Rodrigues (ORCID: 0000-0002-3555-8165)
William B. Hanson Center for Space Sciences
University of Texas at Dallas – UT Dallas
Richardson, TX
fabiano@utdallas.edu

Abstract

This work aims to evaluate the performance of Phase-Locked Loop (PLL) under the presence of distinct scintillation patterns in the signal. Scintillation is very common in low-latitude regions due to the ionospheric dynamics. Under strong scintillation scenario the occurrence of deep fading events is usually registered and may cause severe degradation in the communication. The investigation conducted in this work uses the amplitude scintillation index S_4, the decorrelation time τ_0, and the bandwidth B_n as main parameters. The study evaluates 54 different combinations of these parameters. The results indicate that in order to minimize the occurrence of cycle slips in the output phase of the PLL, the most appropriate tracking loop bandwidth B_n depends on the values of both S_4 and τ_0, which characterize the scintillation fading pattern. Simulations showed that as the S_4 index increases, the automatic increment in the PLL bandwidth may not be the best choice as the performance depends on the temporal characteristics of the scintillating signal. The analysis showed that, among the configurations tested, the equivalent noise bandwidth of 10 Hz achieved the best performance overall. The investigation also showed that choosing the wrong parameter regarding the PLL bandwidth may increase the probability of cycle slip by up to 10 times during fading events.

1. Introduction

Global Navigation Satellite Systems (GNSS) are widely used nowadays and the estimated market for civilian GNSS applications will be near € 135 billion by 2025 (Sanz, 2017). Timing and synchronization, logistics chains, and transportation are examples of GNSS applications. There are also applications, which require centimeter-level precision positioning such as offshore operations and precision agriculture. Those are just a few examples of a technology that is heavily dependent on GNSS. One can also cite the use of satellite navigation to optimize route planning on roads and cities, establishment of optimal routes for supply chain distributions, and logistics applications.

The most commonly used constellation in civilian applications is the Global Positioning System (GPS) from the United States. Currently, GPS provides 3 open carrier frequencies, L1, L2C, and L5.

In the context of aviation, there are some approaches, named augmentation systems, created to enhance the quality of positioning information. One of these methods is the so-called Ground Based Augmentation System (GBAS). GBAS is a local differential GPS approach that broadcasts corrections for commercial aviation. The implementation of GBAS in airports is increasing and expanding worldwide. This system has been designed to provide navigation aid for Category-I (CAT I) precision approach under low visibility conditions. This is an application classified as safety-critical, which can bring a series of benefits, including reduced fuel consumption and reduced CO^2 emission because of the improved air traffic control service.

However, the use of this approach at low latitudes is still a challenge because of the effects of the space plasma environment near Earth that includes the ionosphere. The Earth's ionosphere can be described as a magnetized plasma. Complex physical processes associated with activity in the Sun and in the lower neutral atmosphere cause a large degree of variability in ionospheric plasma. This variability causes a broad range of effects on trans-ionospheric signals, including diffraction and refraction. These effects are more severe during nighttime when large spatial plasma density gradients are created by plasma instabilities, which develop in the lower portion of the ionosphere (bottom side F-region).

These instabilities start at the geomagnetic equator and quickly evolve vertically in the form of the so-called Equatorial Plasma Bubbles (EPBs). These EPBs expand along geomagnetic field lines and often reach latitudes (up to about 20^o) away from the equator. Therefore, the EPBs eventually reach latitudes where the background plasma density is enhanced due to the Fountain Effect (Moraes et al., 2018a). The EPBs have scale sizes varying from a few 10s of km to 100s of km. During its evolution, however, cascading processes cause the development of irregularities with smaller scales sizes. Irregularities with scale sizes of a few 100s of m are responsible for ionospheric scintillations, which is the main subject of this study. Ionospheric scintillations can be described as rapid fluctuations in amplitude and/or phase of trans-ionospheric signals including those used by GNSS. Additional information about scintillation is provided in the following section. Here, we simply illustrate the drastic variations in ionospheric total electron content (TEC) associated with EPBs and observed over the Brazilian sector. Signatures of EPBs can be seen as variations in TEC, transverse to the geomagnetic equator (red line) that can be seen in Figure 1.

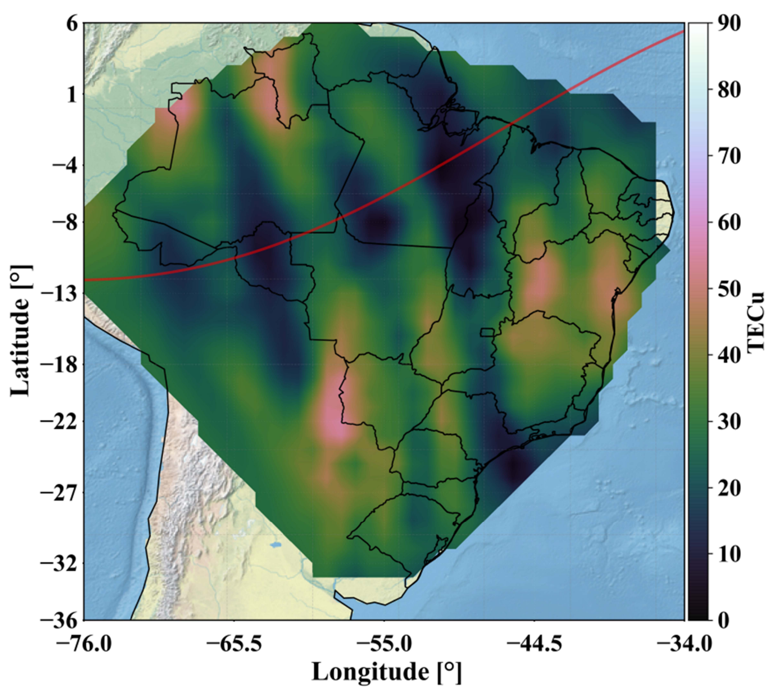

Figure 1: TEC map over Brazilian territory do the night of February 15 2014 at 23:30 LT, showing the large background TEC in the Equatorial Ionization Anomaly (EIA) region and the magnetic aligned EPBs.

Some of these EPB events can lead to loss of integrity for the system corrections. Furthermore, scintillation events associated with EPBs can cause cycle slips and eventually loss-of-lock in GNSS signals, which then may result in potential availability problems for satellite navigation users (Roy and Paul, 2013). Besides spatial gradients, larger in the anomaly crest region (Biswas et al., 2019), the EPBs dynamic features may also play a significant role in the signal outage events (DasGupta et al., 2006); in the present work a simplified simulation approach was adopted to evaluate the fading effects regardless propagation aspects like relative motion between the GPS satellites and ionospheric irregularities or the direction of propagation. Additionally, there are some results indicating that the scintillation onset follows some seasonal patterns (Sousasantos et al., 2018). Therefore, it is important to study the effects of ionospheric scintillation on GNSS receiver performance.

Therefore, the main objective of this study is to characterize the performance of GPS receivers under the effects of ionospheric scintillation. The response of the receiver will be investigated for different scintillation scenarios and by evaluating different receiver parameters. The analysis intents to reveal the settings of the receiver that would make its operation more robust to scintillation events and, therefore, reducing possible availability issues.

The rest of the paper is organized as follow: in section 2 details about the mathematical model of the ionospheric scintillation is presented as well the methodology adopted for simulating the signals. Section 3 describes the Phase-Locked Loop (PLL) model used in this work; this section also shows the validation of the implemented model and the system performance metric, which is the cycle slip. In section 4 the results of PLL performance based on various simulation scenarios are presented. This section also shows the best PLL configuration according to the scintillation characteristic. Special attention is paid to analyzing the probability of cycle slip during fading events. Finally, section 5 summarizes the findings of this work.

2. Ionospheric Scintillation

Ionospheric scintillation is one of the effects of space weather conditions, and it can be described as rapid phase and/or amplitude fluctuations in radio signals that propagated through irregularities in the ionospheric plasma (Kintner et al., 2007). It occurs more often and more severely in the low-latitude region during equinoxes for most longitude sectors (Muella et al., 2017).

The GNSS/GPS signal is vulnerable to this effect and scintillations can cause degradation in positioning or even interruptions in the system availability (Conker et al., 2003). The degradation in positioning can be related to pseudo-range errors introduced by the loss-of-lock in one or more of the channels simultaneously, which may increase dilution of precision. In more severe cases, when there are losses-of-lock in several channels, simultaneously, positioning can be interrupted, but these extreme cases are beyond the scope of the present work.

A channel under the effects of the ionospheric scintillation can be modeled as a multiplicative channel (Humphreys et al., 2010):

$$y(t) = z(t)\, s(t) + n(t), \qquad (1)$$

where y(t) is the complex envelope of the received signal, s(t) is the complex envelope of the transmitted signal, z(t) is the complex channel response, and n(t) is an additive noise. The channel response z(t) is composed of the amplitude and phase of the scintillation as:

$$z(t) = \rho_s(t)\ exp\,[j\theta_s(t)], \qquad (2)$$

where $\rho_s(t)$ represents amplitude scintillation and $\theta_s(t)$ represents phase scintillation. Both, amplitude $\rho_s(t)$ and phase $\theta_s(t)$ scintillation, are stochastic processes. Earlier studies assumed the amplitude $\rho_s(t)$ to follow a Nakagami-*m* distribution (e.g., Fremouw et al., 1978; Banerjee et al., 1992). More recently, Humphreys et al. (2010) justified the use of the Rice model and Moraes et al. (2013) validated the use of the α-μ model. Additionally, Moraes et al. (2019), showed that the κ-μ model to be another feasible option for modeling amplitude scintillation. The phase, $\theta_s(t)$, on the other hand, is assumed to follow a zero-mean Gaussian distribution according to Hegarty et al. (2001).

Common parameters to indicate the severity of the scintillation are the S_4 index and the channel decorrelation time τ_0. The S_4 index is related to the strength of the amplitude scintillation and the depth of the fading events (i.e., events when the signal intensity drops steeply). It can be calculated by (Yeh and Liu, 1982):

$$S_4 = \sqrt{\frac{E({\rho_s}^4) - E({\rho_s}^2)^2}{E({\rho_s}^2)^2}}, \quad (3)$$

where $E(\cdot)$ represents the expected value. Values close to 0 indicate the absence of scintillation, whereas values close to 1 indicate a severe event of amplitude scintillation. The empirical calculation of S_4 is usually computed for measurements made over a period of 60 s (Kintner et al., 2007).

Panels (a) and (b) from Figure 2 show two examples of scintillating signals with $S_4 = 0.71$ and $S_4 = 0.86$, respectively. The example in panel (b) shows a more severe scintillation event, with the occurrence of deeper fading events in signal intensity.

The decorrelation time τ_0 is related to the fading rate and its duration. Formally, the τ_0 is defined as the time lag (τ) for which the autocorrelation function ($R_\xi(\tau)$) of the time varying component ($\xi(t)$) of the scintillation complex response $z(t)$ falls off by a factor of $1/e$ (Humphreys et al., 2010), or equivalently:

$$\frac{R_\xi(\tau_0)}{R_\xi(0)} = e^{-1}. \quad (4)$$

To exemplify the concept of this parameter, the panels (a) and (b) of Figure 2 have $\tau_0 = 0.40$ s and $\tau_0 = 1.00$ s, respectively. It can be seen that the signal of panel (a) has a higher fading rate (smaller τ_0) compared to the signal in panel (b) while showing deeper fades.

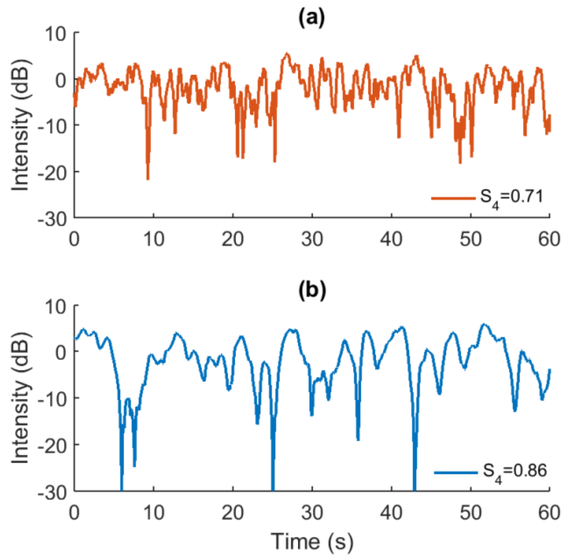

Figure 2: (a) Synthetic amplitude scintillation for $S_4 = 0.71$ and $\tau_0 = 0.40$ s. (b) Synthetic amplitude scintillation for $S_4 = 0.86$ and $\tau_0 = 1.00$ s. Synthetic scintillation patterns were generated using the Humphreys et al. (2009) model.

The objectives of the present work led to employ synthetic scintillation data. Synthetic scintillation allows us to have control over the desired characteristics of the amplitude and phase of the received signal. In this work, the simulation was performed based on the model of Humphreys et al. (2009) and available in: https://gps.ece.cornell.edu/tools.php.

Based on measured time series of scintillation, Humphreys et al. (2009) derived a model capable of generating scintillation patterns. The model assumes a Rice distribution for amplitude scintillation. More importantly, the simulator uses S_4 and τ_0 as inputs. Additionally, the spectrum of a complex scintillating signal is assumed to be shaped by a 2^{nd} order low-pass Butterworth filter where the cutoff frequency is adjusted according to τ_0, and this filter is driven by a stationary zero-mean complex white Gaussian noise. Then, a direct component, which is a constant value, is calculated according to S_4 and is added to a filtered noise. Finally, the result is normalized by its mean value to produce the synthetic scintillation time series z(t). This formulation is applicable to strong scintillation events as discussed in Humphreys et al. (2009), where the authors show the agreement between synthetic and observed scintillation data, particularly with respect to spectral features, i.e. second order statistics. As mentioned earlier, this synthetic simulator generates a time series that follows a Rice distribution, which is a fair first order statistical model, as discussed in Moraes et al., (2019). Other simulators could be employed such as the Nakagami-m presented by Santos Filho et al., (2007) or the α-μ based from Gherm and Zernov (2015). Those models, however, are not directly related to the parameter τ_0 but they obviously are capable of generating the correlated time series obeying prescribed autocorrelation coefficients and therefore they surely can be characterized by the parameter τ_0.

In this paper, this model will be applied to generate synthetic scintillating signals to evaluate the tolerance of a Phase-Locked Loop (PLL) system under varying scintillation conditions. Figure 3 shows one example of both amplitude and phase from scintillation-simulated data.

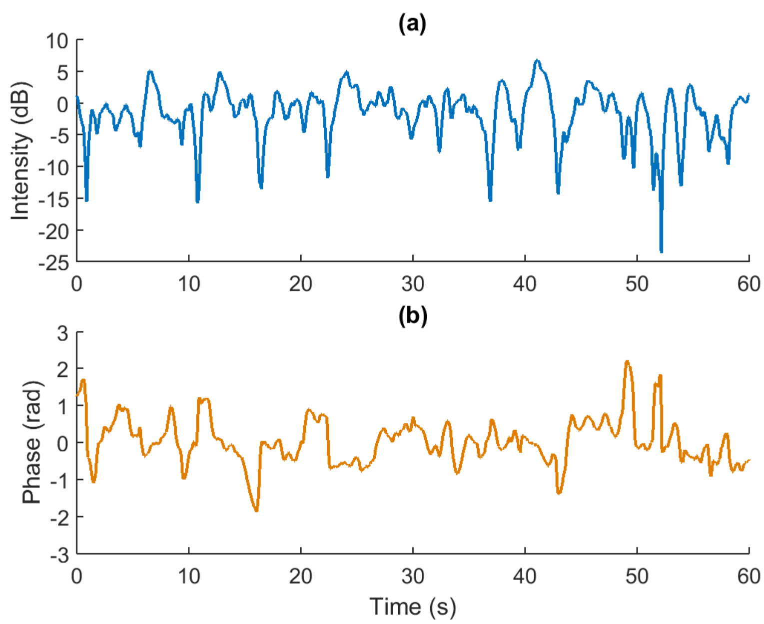

Figure 3: Synthetic scintillation data generated. (a) Amplitude scintillation with S_4 = 0.8 and τ_0 = 0.4 s. (b) The respective simulated phase scintillation.

3. PLL Tracking loop model

Carrier synchronization is a fundamental part of the GNSS receiver and it is usually composed of two steps: acquisition and tracking (Kaplan and Hegarty, 2005). While the first is responsible for detecting the presence of a given GNSS satellite signal and providing a coarse estimate of the synchronization parameters, the latter is responsible of keeping track of these signals and refining the estimation of the parameters. The conventional method of GNSS carrier tracking is based on the Phase-Locked Loop (PLL).

The input of the carrier tracking loop can be considered as the output of the prompt correlator that performs the synchronization of the pseudorandom code. In the presence of the ionospheric scintillation, the complex envelope of this input y_k can be expressed as:

$$y_k = \rho_{s,k}\, \alpha_k\;\; exp\,(j[\theta_k + \theta_{s,k}]) + \eta_k, \tag{5}$$

where $\rho_{s,k}$ and $\theta_{s,k}$ are the scintillation amplitude and phase, respectively, α_k and θ_k are the amplitude and phase of the input signal and η_k is an additive noise. The sample rate of these variables is defined by the integration time of the correlators T, which varies from 1 to 20 ms for the GPS L1 C/A signal, for example. The additive noise η_k is considered to have a zero mean Gaussian distribution with σ_η^2 variance. The carrier-to-noise density ratio (C/N_0) of the input signal is defined by α_k, σ_η^2 and T using the expression $C/N_0 = {\alpha_k}^2/(2\,T\,{\sigma_\eta}^2)$.

It is desired that the carrier tracking loop estimates the carrier phase θ_k, but as a consequence the scintillation phase $\theta_{s,k}$ is also estimated. Then, the output of PLL, $\hat{y}_k$, can be expressed as:

$$\hat{y}_k = exp\,(-j[\hat{\theta}_k + \hat{\theta}_{s,k}]), \tag{6}$$

where $[\hat{\theta}_k + \hat{\theta}_{s,k}]$ is the joint estimate of the signal and scintillation phases. With the feedback of this output, it is possible to obtain an error signal from the input by using an arctangent phase discriminator given by:

$$e_k = tan^{-1}\,[Im(y_k \cdot\; \hat{y}_k)\,/\,Re(y_k \cdot\; \hat{y}_k)]. \tag{7}$$

The error signal e_k is filtered by a loop filter, which determines the order of the PLL, and then is integrated by the Numerically-Controlled Oscillator (NCO). For the first, second and third-order PLL, the loop filter and NCO combined transfer function in the Laplace transform domain is given respectively by (Ward et al., 2006):

$$F_1(s)\,N(s) = \frac{\omega_n}{s}, \tag{8}$$

$$F_2(s)\,N(s) = \sqrt{2}\,\frac{\omega_n}{s} + \frac{{\omega_n}^2}{s^2}, \tag{9}$$

$$F_3(s)\,N(s) = 2.4\,\frac{\omega_n}{s} + 1.1\,\frac{{\omega_n}^2}{s^2} + \frac{{\omega_n}^3}{s^3}, \quad (10)$$

where ω_n is the natural frequency of the loop. These combined transfer functions relate the estimated output phase to the error signal. To implement these transfer functions in the discrete-time domain, the transformation $s = (1 - z^{-1})/T$ is considered, which an approximation of the integral by a rectangle.

An important parameter in the PLL performance is the equivalent noise bandwidth B_n, which can be calculated for the first, second and third-order PLL, respectively by (Ward et al., 2006):

$$B_{n,1} = 0.25\,\omega_n, \quad (11)$$

$$B_{n,2} = 0.53\,\omega_n, \quad (12)$$

$$B_{n,3} = 0.7845\,\omega_n. \quad (13)$$

As the equivalent noise bandwidth is a function of the natural frequency, B_n can be chosen by tuning ω_n in the transfer function of the loop filter. Higher values of B_n imply a faster response to dynamic input, but also imply a noisier response.

The resulting block diagram of the PLL model implemented in this research is shown in Figure 4 with the elements described above.

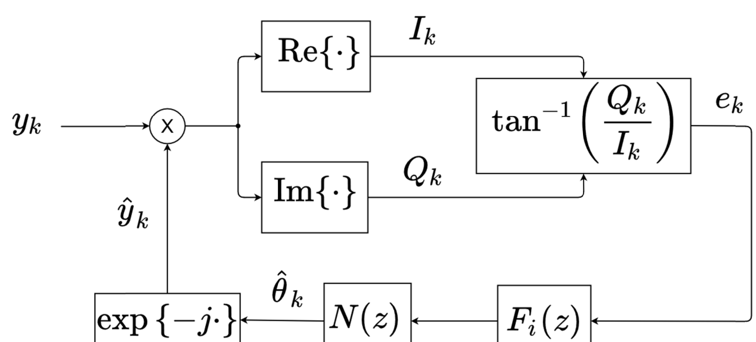

Figure 4: Block diagram of the PLL model considered.

The standard deviation measured in the output phase can be compared with its expected analytical value, given by (Holmes, 1982):

$$\sigma_{\hat{\theta}} = \frac{180}{\pi}\sqrt{\frac{B_n}{C/N_0}\left(1+\frac{1}{2\,T\,C/N0}\right)} \quad [degree]. \tag{14}$$

Equation (14) was used for validating the PLL implementation. Considering C/N_0 ranging from 30 to 50 dB-Hz in the absence of scintillation, a second order PLL with 1 ms integration time and the equivalent noise bandwidth values of 5, 10 and 15 Hz, Figure 5 shows the agreement of the considered PLL model with the theoretical curves.

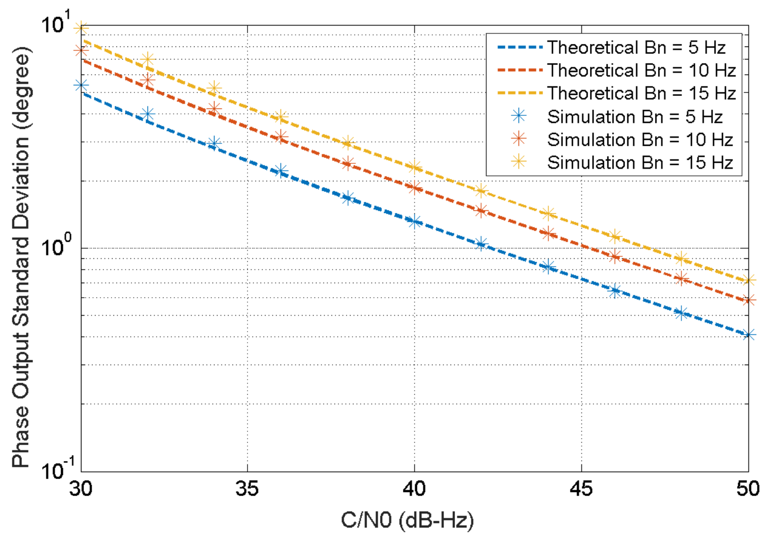

Figure 5: Output phase standard deviation in the absence of scintillation: simulation measure vs. theoretical value.

The arctangent phase discriminator considered in this paper is periodic and cannot distinguish phase errors of φ and $\varphi + 180 \times n$, $(n \in Z)$. Then, at low C/N_0 or during a strong ionospheric scintillation scenario, where the standard deviation of the phase error increases, the phase error can slip from one integer level n to another. This phenomenon is known as cycle slip and it can lead the output phase to a stationary error not perceived by the PLL. A consequence of several successive cycle slips at once is the internal frequency estimate of the loop filter falling of the frequency pull-in range, which results in a loss-of-lock (Humphreys et al., 2005). It is important to emphasize that the loss-of-lock and the cycle slips are related, but they are different events. While the cycle slip is characterized by slips of multiples of 180 degrees in the phase error, in which the PLL may eventually maintain its locked state, the loss-of-lock is a more severe event characterized by a varying phase error and a frequency error different from zero, in which the PLL is not in steady state. Figure 6 shows an example of phase error obtained through the synthetic scintillation data processed by the PLL model. In this case, the loop had been stressed to force the occurrence of cycle slips. It can be seen a total of 4 cycle slips in this example, where the error transits between -180, 0 and 180 degrees.

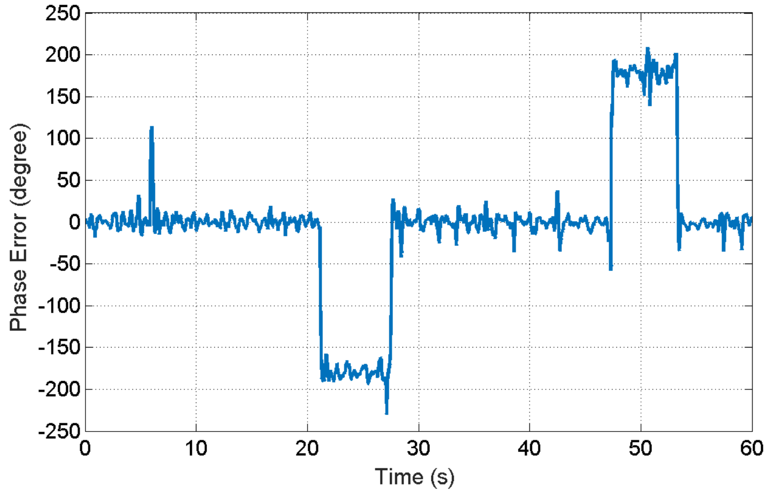

Figure 6: Example of cycle slip occurrence in the phase error in the presence of scintillation.

In this work, the parameter selected for performance evaluation was the mean time between cycle slips. This parameter cannot be obtained based on a linear model of the PLL, which means the average time that a phase error transitions between -180, 0 and 180 degrees needs to be treated based on results from nonlinear models. For a first order PLL, the mean time between cycle slips is given by (Viterbi, 1966):

$$T_S = \frac{\pi^2 \rho I_0^2(\rho)}{2B_n} \quad [s], \tag{15}$$

where $\rho = \frac{1}{4\sigma_{\hat{\theta}}{}^2}$ is the signal-to-noise ratio for the Costas loop (Knight 2001) and $I_0(\cdot)$ is the modified Bessel function of first kind and zeroth order. It is important to note that the result of equation (15) is obtained for a first-order PLL, and a closed expression for a 2nd order loop is not available. Holmes (1971) and Sanneman and Rowbotham (1964) both estimated mean time between cycle slips for 2nd order loop based on simulations. Their results showed lower values of mean time between cycle slips in this case. Holmes (1982) suggested that this performance is approximated to the first order but with 1 dB less in the ρ. Obviously, these results do not include disturbances such as phase and amplitude scintillation.

Under conditions of strong fading events and low C/N_0 (i.e. noisy conditions) the occurrence of cycle slips becomes recurrent. The time between the occurrence of cycle slips is an unknown measure under different ionospheric scintillation, that is varying S_4 index and decorrelation time τ_0. So it is interesting to characterize the receiver performance under different equivalent noise bandwidth B_n in the PLL. This is the subject of next section.

4. Evaluation of receiver performance

It is important to map the receiver performance under scintillation to verify which configuration can make it less susceptible to the effects of the ionosphere. In this section, a series of simulations will be carried out to investigate receiver performance as function of equivalent noise bandwidth B_n , having as metric the mean time between cycle slips.

The procedure adopted in this evaluation consists in the generation of a set of scintillation time series, varying the value of S_4 from 0.5 to 1.0 and τ_0 from 0.2 to 1.0 s. The chosen S_4 values are justified because this is the range in which the receiver will have the highest tracking error estimates according to Moraes et al. (2014). Also, because these scenarios are more susceptible to the occurrence of cycle slips as shown by Moraes et al. (2011). The synthetic scintillation data were generated according to the methodology described in section 2, based on the simulator from Humphreys et al. (2009).

The PLL tracking loop, based on the Costas model was implemented, and the synthetic scintillation was applied in the model according to equation (5). In all tests performed, the C/N_0 was adjusted to 45 dB-Hz. Regarding the integration time, higher values are preferable in order to reduce the standard deviation of the output phase, as seen in equation (14), and the value T = 10 ms was chosen, because it leads the PLL to a better performance than the value T = 20 ms, according to Humphreys et al. (2010). The receiver was a 2nd order PLL, this choice had been made because, according to Holmes (1982), third order PLL has inherent stability issues due to the gain of the filter. The simulations were performed considering four equivalent noise bandwidths B_n, the values were 2, 5, 10 and 15 Hz.

Narrower values of B_n correspond to smaller values of $\sigma_{\hat{\theta}}$. On the other hand, narrow B_n can make PLL cycle slip occurrences more frequent (Holmes, 1982), and according to Guo et al. (2020) low values of B_n increase phase scintillation induced tracking jitter. Therefore, these B_n values will be evaluated to see which configuration presents the best performance, according to the tested scintillation scenario.

For each combination of S_4 and τ_0, a total of 10 hours of scintillation was generated and run. The synthetic signal provided total control of the simulation, thus knowing the real value of the received phase and when there would be cycle slips. Figure 7 shows one example of the cumulative cycle slip events observed for the simulations with $S_4 = 0.9$ and $\tau_0 = 0.3$ s for $B_n = 2$, 5, 10 and 15 Hz. In this particular simulation, the configuration with $B_n = 2$ Hz, recorded a total of 13,698 occurrences of cycle slips over the 10 hours. This is the worst performance in this particular scintillation condition. In this scenario, the best performance was achieved by the PLL with $B_n = 15$ Hz, with only 4790 occurrences of cycle slips, a reduction of approximately 65% in this kind of failure in the receiver operation.

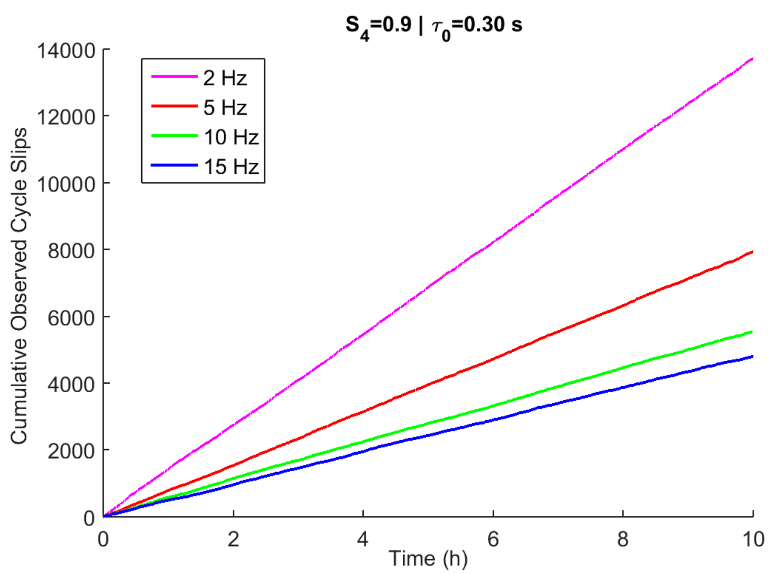

Figure 7: Cumulative records of cycle slip occurrences during 10 hours of simulation for different PLL equivalent noise bandwidths (B_n). Values of $S_4 = 0.9$ and $\tau_0 = 0.3$ s were used.

The mean time between cycle slips here is assumed as the period of simulation (10 hours) divided by the total number of slips. The scintillation environment was evaluated for $S_4 = 0.5$ up to 1.0 in intervals of 0.1. The decorrelation time τ_0 was tested on the range between 0.2 to 1.0 s with time span of 0.1 s. These conditions generated a set of 54 combinations that were simulated with the four values of B_n aforementioned, totaling 216 experiments. While the strength of the scattering is related to the S_4 level, the decorrelation time describes the spectrum characteristics; hence, both parameters are required to evaluate the PLL performance. Figure 8 shows the results of the simulations. Each panel represents one S_4 value and the mean time between cycle slip are presented as function of τ_0 for B_n = 2, 5, 10 and 15 Hz. As expected, the mean time between cycle slips decreases according to the increase in the value of S_4. Considering a given fixed value of S_4 (i.e., one panel), the influence of the τ_0 parameter is noticeable. For example, taking S_4 = 0.8 and $\tau_0 = 0.2$ s, while B_n = 2 Hz presents a mean time of 2.92 s, for B_n = 15 Hz the respective value is 8.12 s. Still considering S_4 = 0.8 but analyzing now τ_0 =1.0 s, for the values of B_n of 2 Hz and 15 Hz, the mean time will be respectively 30.23 and 30.74 s. These examples and its variation in the values shows how the scintillation pattern for the same S_4 can affect the performance of the receivers. This example also shows that depending on the B_n value adopted, the mean time can vary at a rate up to 3.5 times for the same S_4. In other words, properly chosen B_n settings can significantly improve the functioning of the receptor under the effects of scintillation. Indeed, in this aforementioned scenario (S_4 = 0.8, τ_0 =0.2 s), for a PLL equivalent noise bandwidth of 10 Hz the mean time between cycle slips would be approximately 45 s. This is an improvement of approximately 50%, this example shows how important is the proper configuration of the receiver according to the scintillation environment experimented by the user.

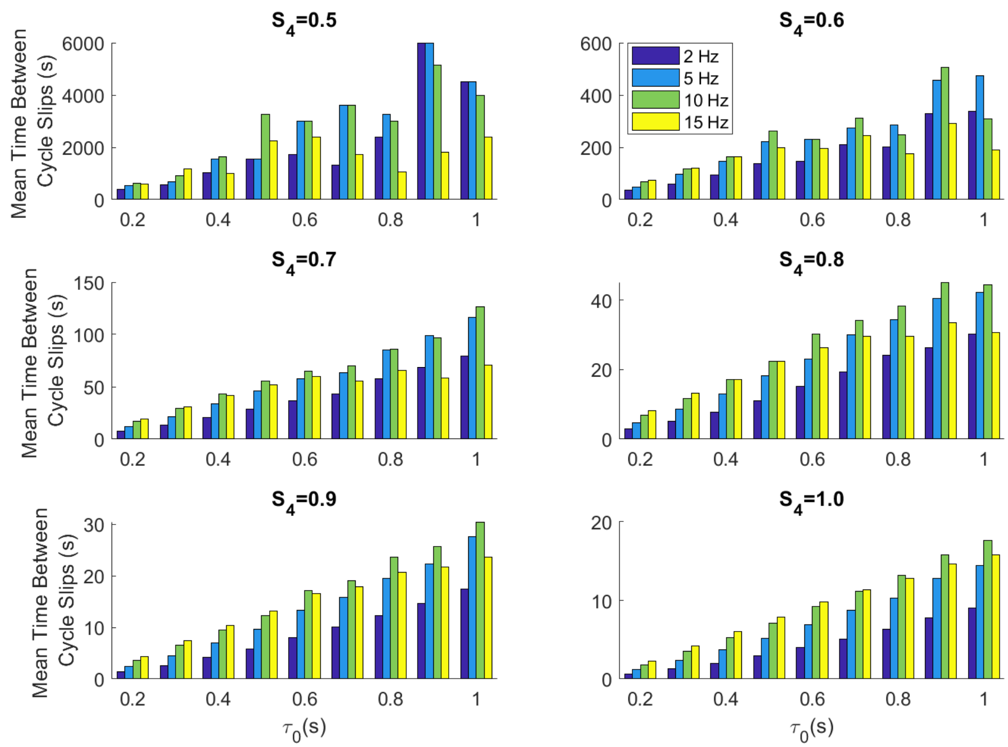

Figure 8: Mean time between cycle slips for different simulated scintillation scenarios, showing the influence of the B_n value on the performance of the PLL.

Complementing this analysis, Figure 9 exhibits a matrix with the tested S_4 and τ_0 values, showing the receiver equivalent noise bandwidth setting with the highest mean time value between cycle slips in each of the simulations. Figure 9 shows that, for strong scintillation values in the range of $0.5 \leq S_4 < 0.8$, the best performance will depend on the decorrelation time. For $\tau_0 < 0.5$ the value of B_n = 15 Hz obtained the best result. For $\tau_0 \geq 0.8$ s the choice of B_n = 5 Hz is the most recommended, and in the middle of the range B_n = 10 Hz would be the most appropriate. As the scintillation reaches very strong levels (e.g. $S_4 \geq 0.8$) the choice of B_n = 5 Hz is no longer adequate due to the low mean time values obtained. For S_4 = 0.8, if $\tau_0 \leq 0.4$ s, the best performance was found with B_n = 15 Hz, outside this range, B_n = 10 Hz was the best result. As S_4 increases the choice of B_n = 15 Hz, it becomes the best choice even for signals with higher τ_0 values. Figure 9 also shows in red dashed line the average values of τ_0 reported by Moraes et al. (2012) in São José dos Campos, the peak of EIA under maximum solar flux conditions. Based on such results, for the evaluated range of scintillation, the choice of B_n = 10 Hz seems to be the most appropriate for scenarios where $S_4 < 0.8$ and above this index, B_n = 15 Hz presents the best performance, thus being the most recommended for these more severe cases.

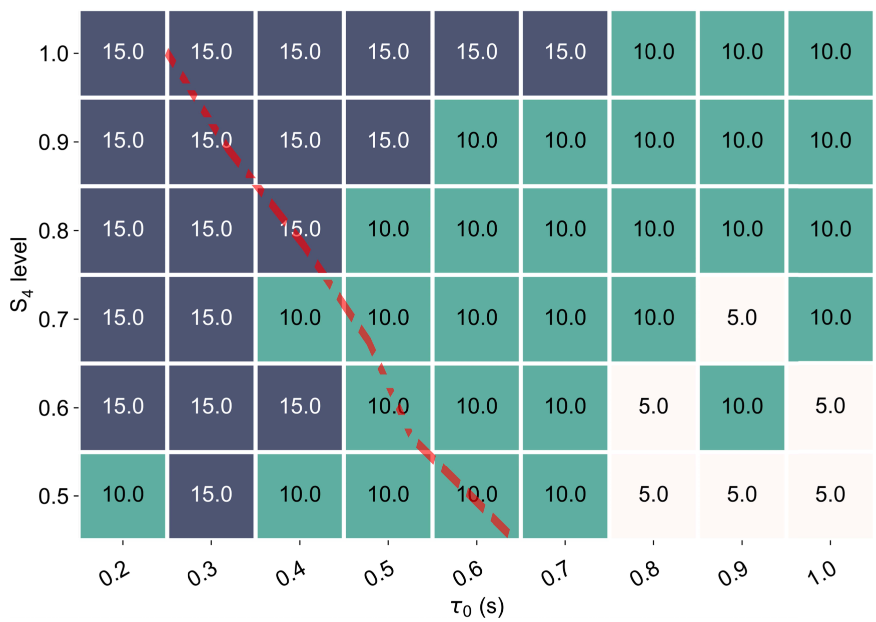

Figure 9: Equivalent noise bandwidth (B_n) in the PLL that achieved the best results in the simulations considering different scintillation scenarios. The red dashed line shows the typical values of τ_0 found in the literature.

Another aspect that deserves attention is the tolerance of the loop to fading events. Most cycle slips occur during these events, so it is interesting to analyze how the PLL responds according to the B_n setting, during fading events. During simulations, all fading events were recorded and then the empirical probabilities of a cycle slip as a function of the fading depth were computed. Figure 10 shows the statistics of these events. For example, considering S_4 = 1.0 and τ_0= 0.8 s, in this simulation scenario for B_n = 10 Hz, during a fading event of -10 dB (in depth), the probability of a cycle slip occurring was 6.7%. For same S_4 = 1.0 but with τ_0= 0.4 s and the same value of B_n, taking the same threshold of -10 dB (in depth), the probability increased to 60.5%. Analyzing Figure 10, it is possible to note that fading events deeper than - 15 dB becomes critical for the receiver. This is especially true as the τ_0 value decreases because of the probability of cycle slips increases significantly. According to the analysis of Moraes et al. (2018b), events with - 15 dB are very likely to occur in the EIA peak region, therefore, a properly configured receiver is very important under these circumstances. Carrano and Groves (2010) also showed that scenarios with higher values of S_4 and decreased τ_0 result in greater chances of losing lock. This is due to the fact that the lower τ_0 causes a higher fading rate and, consequently, a greater probability of having fading events below -15 dB, which the simulations showed as a critical threshold for loop operation. It is worth noting that choosing a suitable B_n will make the receiver more tolerant to fading events. For severe scintillation though, the results indicate that a very narrow B_n can cause excessive cycle slips to occur during fading events.

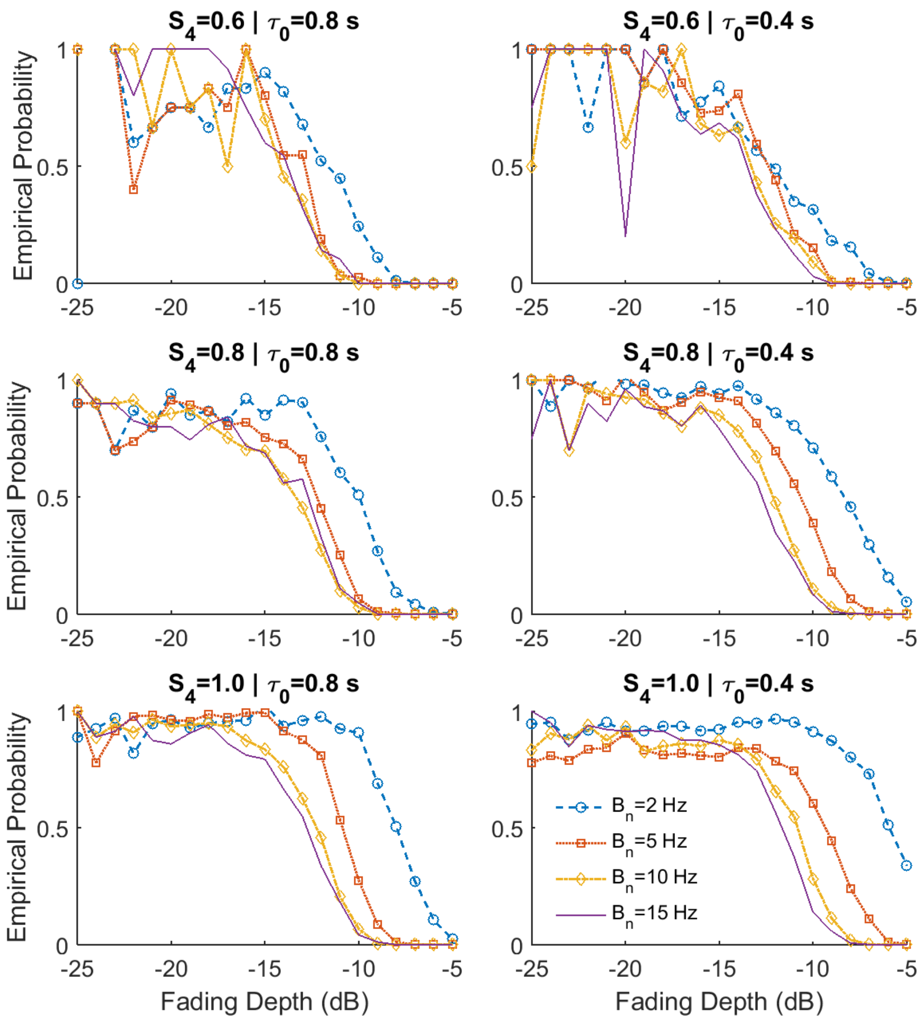

Figure 10: Empirical probability of cycle slip as function of fading event depth for different values of S_4 and τ_0 considering B_n = 2, 5, 10 and 15 Hz.

5. Summary and Conclusions

The increase number of applications that depend on GNSS information is a reality in many areas. The signals used by GNSS, however, must travel through the ionospheric region, which can be described as a magneto-ionized plasma environment. At low-latitude regions in particular, the complex dynamics of the plasma environment can severely affect the propagation of GNSS signals. Large ionospheric density gradients and irregularities associated with EPBs can affect trans-ionospheric signals, by causing delays, changes in the signal amplitude and phase, which producing ionospheric scintillation. During scintillation, deep fading events can occur leading to an increased probability of cycle slips, loss-of-lock, etc. These problems might cause several safety and financial losses and, therefore, it is important to investigate mitigation strategies to overcome the effects of scintillation. One possible approach, which is employed in this study, is to use synthetic scintillation patterns and a PLL algorithm to determine the effects of different scintillation patterns on the PLL and to evaluate optimal PLL parameters.

This work evaluates the PLL loop response for several different scintillation environments, which were parameterized in the simulations using commonly used scintillation parameters, namely the amplitude scintillation index S_4 and the decorrelation time τ_0. A total of 54 different scintillation scenarios were investigated, which allowed us to verify the role of each scintillation parameter on PLL performance.

The simulations showed that a proper choice of the equivalent noise bandwidth (B_n) in the GNSS receiver is essential for users operating under such harsh condition. A proper choice of B_n will make the receiver more robust to scintillation-related fadings. For severe scintillation it is seen that a very narrow B_n (say, 2 Hz) can cause excessive cycle slips during fading events. When looking at the overall results, it can be observed that as the S_4 index increases, wider B_n are preferred for a better tracking performance. And, as the decorrelation time τ_0 increases, a narrower B_n becomes more appropriate. So, a proper choice of the equivalent noise bandwidth will depend on both scintillation parameters S_4 and τ_0, as shown in Figure 10. But when considering a fixed B_n to be set in a GNSS receiver, it can be seen that $B_n = 10$ Hz would have the best overall performance among the candidates (2, 5, 10 and 15 Hz) evaluated in this study.

Acknowledgements: IPP performed this research in the framework of the INCT GNSS-NavAer, CNPq 465648/2014-2 and FAPESP 2017/50115-0. AOM is supported by CNPq award number 314043/2018-7. J. Sousasantos acknowledges FAPESP for the financial support under process 2018/06158-9. F. S. Rodrigues would like to thank support from NSF (AGS-1916055). Datasets for this research are available for download at the following link: https://zenodo.org/record/3912019#.XvqC9ShKjI

References

Biswas, T., Ghosh, S., Paul, A., & Sarkar, S. (2019). Interfrequency performance characterizations of GPS during signal outages from an anomaly crest location. *Space Weather*, *17*(6), 803-815.

Carrano, C. S., & Groves, K. M. (2010). Temporal decorrelation of GPS satellite signals due to multiple scattering from ionospheric irregularities. In Proceedings of the 23rd International Technical Meeting of The Satellite Division of the Institute of Navigation (ION GNSS 2010) (pp. 361-374). Manassas, Va.: Inst. of Navig.

Conker, R. S., El-Arini, M. B., Hegarty, C. J., & Hsiao, T. (2003). Modeling the effects of ionospheric scintillation on GPS/satellite-based augmentation system availability. *Radio Science*, *38*(1).

DasGupta, A., Paul, A., Ray, S., Das, A., & Ananthakrishnan, S. (2006). Equatorial bubbles as observed with GPS measurements over Pune, India. *Radio science*, *41*(05), 1-11.

Gherm, V. E., & Zernov, N. N. (2015). Strong scintillation of GNSS signals in the inhomogeneous ionosphere: 2. Simulator of transionospheric channel. *Radio Science*, *50*(2), 168-176.

Guo, K., Aquino, M., & Vadakke Veettil, S. (2019). Effects of GNSS receiver tuning on the PLL tracking jitter estimation in the presence of ionospheric scintillation. *Space Weather*, e2019SW002362.

Hegarty, C., El-Arini, M. B., Kim, T., & Ericson, S. (2001). Scintillation modeling for GPS-wide area augmentation system receivers. *Radio Science*, *36*(5), 1221-1231.

Holmes, J. (1971). First slip times versus static phase error offset for the first-and passive second-order phase-locked loop. *IEEE Transactions on Communication Technology*, *19*(2), 234-235.

Holmes, J. K. (1982). *Coherent spread spectrum systems*. John Wiley & Sons.

Humphreys, T. E., Psiaki, M. L., & Kintner, P. M. (2005). GPS carrier tracking loop performance in the presence of ionospheric scintillations. In *Radionavigation Laboratory Conference Proceedings*.

Humphreys, T. E., Psiaki, M. L., Hinks, J. C., O'Hanlon, B., & Kintner, P. M. (2009). Simulating ionosphere-induced scintillation for testing GPS receiver phase tracking loops. *IEEE Journal of Selected Topics in Signal Processing*, *3*(4), 707-715.

Humphreys, T. E., Psiaki, M. L., Ledvina, B. M., Cerruti, A. P., & Kintner, P. M. (2010). Data-driven testbed for evaluating GPS carrier tracking loops in ionospheric scintillation. *IEEE Transactions on Aerospace and Electronic Systems*, *46*(4), 1609-1623.

Kaplan, E., & Hegarty, C. (2005). *Understanding GPS: principles and applications*. Artech house.

Kintner, P. M., Ledvina, B. M., & De Paula, E. R. (2007). GPS and ionospheric scintillations. *Space weather*, *5*(9).

Moraes, A. O., da Silveira Rodrigues, F., Perrella, W. J., & de Paula, E. R. (2012). Analysis of the characteristics of low-latitude GPS amplitude scintillation measured during solar maximum conditions and implications for receiver performance. *Surveys in geophysics*, *33*(5), 1107-1131.

Moraes, A. O., Costa, E., de Paula, E. R., Perrella, W. J., & Monico, J. F. G. (2014). Extended ionospheric amplitude scintillation model for GPS receivers. *Radio Science*, *49*(5), 315-329.

Moraes, A. D. O., Vani, B. C., Costa, E., Abdu, M. A., de Paula, E. R., Sousasantos, J., ... & Shimabukuro, M. H. (2018a). GPS availability and positioning issues when the signal paths are aligned with ionospheric plasma bubbles. *GPS Solutions*, *22*(4), 95.

Moraes, A. D. O., Vani, B. C., Costa, E., Sousasantos, J., Abdu, M. A., Rodrigues, F., ... & Monico, J. F. G. (2018b). Ionospheric scintillation fading coefficients for the GPS L1, L2, and L5 frequencies. *Radio Science*, *53*(9), 1165-1174.

Moraes, A., Sousasantos, J., de Paula, E. R., da Cunha, J. J. P. P., Lima Filho, V. C., & Vani, B. C. (2019). Performance analysis of κ-μ distribution for Global Positioning System (GPS) L1 frequency-related ionospheric fading channels. *Journal of Space Weather and Space Climate*, *9*, A15.

Muella, M. T., Duarte-Silva, M. H., Moraes, A. O., de Paula, E. R., de Rezende, L. F., Alfonsi, L., & Affonso, B. J. (2017). Climatology and modeling of ionospheric scintillations and irregularity zonal drifts at the equatorial anomaly crest region. In Annales Geophysicae, 35, 1201-1218.

Roy, B., & Paul, A. (2013). Impact of space weather events on satellite-based navigation. Space Weather, 11(12), 680-686.

Sanneman, R. W., & Rowbotham, J. R. (1964). Unlock characteristics of the optimum type II phase-locked loop. *IEEE Transactions on Aerospace and navigational Electronics*, (1), 15-24.

Santos Filho, J. C. S., Yacoub, M. D., & Fraidenraich, G. (2007). A simple accurate method for generating autocorrelated Nakagami-m envelope sequences. *IEEE Communications Letters*, *11*(3), 231-233.

Sanz, I. 2017. GPS, Glonass y Galileo compiten por un mercado de más de 135.000 millones de euros; http://www.infoespacial.com/es/2017/07-/25/noticia-navegacion -europea-frente-glonass.html

Sobral, J.H.A., M.A. Abdu, H. Takahashi, M.J. Taylor, E.R. dePaula, C.J. Zamlutti, M.G. deAquino, and G.L. Borba, Ionospheric plasma bubble climatology over Brazil based on 22 years (1977-1998) of 630 nm airglow observations, J. Atmos. Solar-Terr. Phys., 64, 1517- 1524, 2002, doi: 10.1016/S1364-6826(02)00089-5.

Sousasantos, J., Oliveira Moraes, A. D., Sobral, J. H., Muella, M. T., Paula, E. R. D., & Paolini, R. S. (2018). Climatology of the scintillation onset over southern Brazil. In *Annales Geophysicae* (Vol. 36, No. 2, pp. 565-576). Copernicus GmbH.

Viterbi, A. J. (1966). Principles of coherent communication. McGraw-Hill.

Ward, P. W., Betz, J. W., Hegarty, C. J., & Kaplan, E. D. (2006). Satellite signal acquisition, tracking, and data demodulation. *Understanding GPS: principles and applications*, 153-241.

Yeh KC, Liu CH (1982) Radio wave scintillations in the ionosphere. Proceedings of the IEEE, 70(4):324-360, doi:10.1109/PROC.1982.12313.

Figure 1.

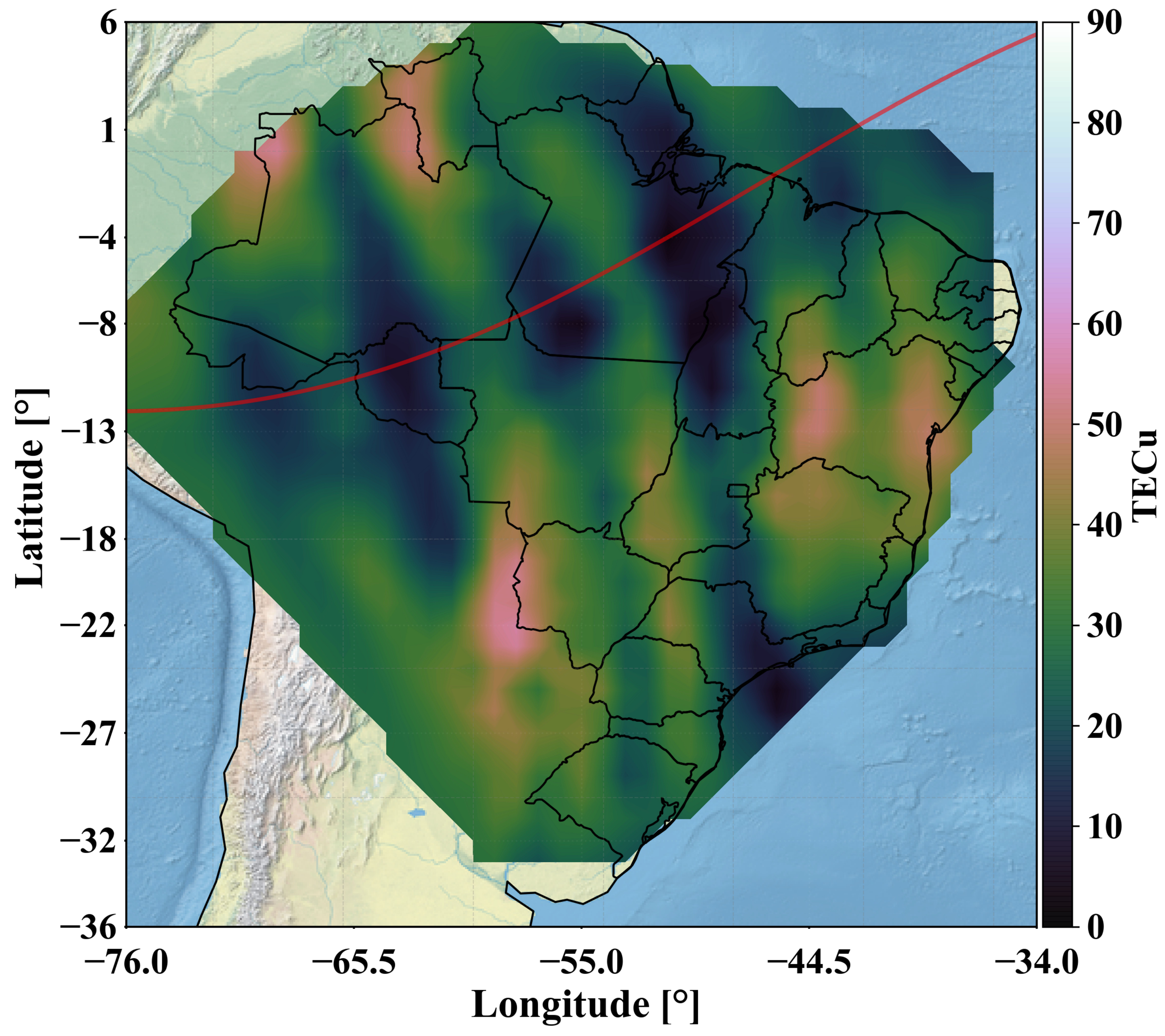

Latitude [°]
Longitude [°]
TECu
6
1
−4
−8
−13
−18
−22
−27
−32
−36
−76.0
−65.5
−55.0
−44.5
−34.0
0
10
20
30
40
50
60
70
80
90

Figure 2.

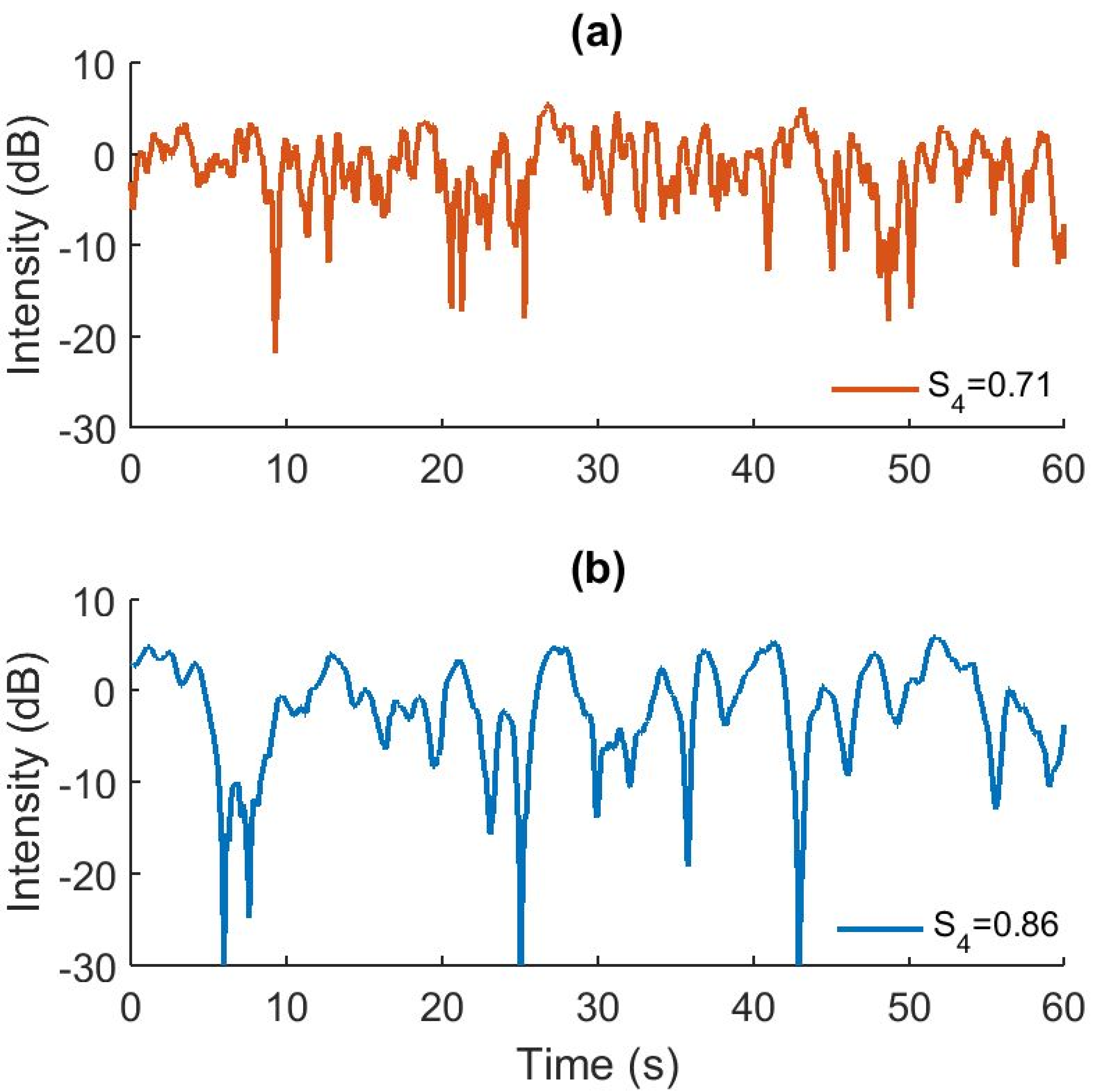
(a)
Intensity (dB)
10
0
-10
-20
-30
0
10
20
30
40
50
60
S4=0.71
(b)
Intensity (dB)
10
0
-10
-20
-30
0
10
20
30
40
50
60
Time (s)
S4=0.86

Figure 3.

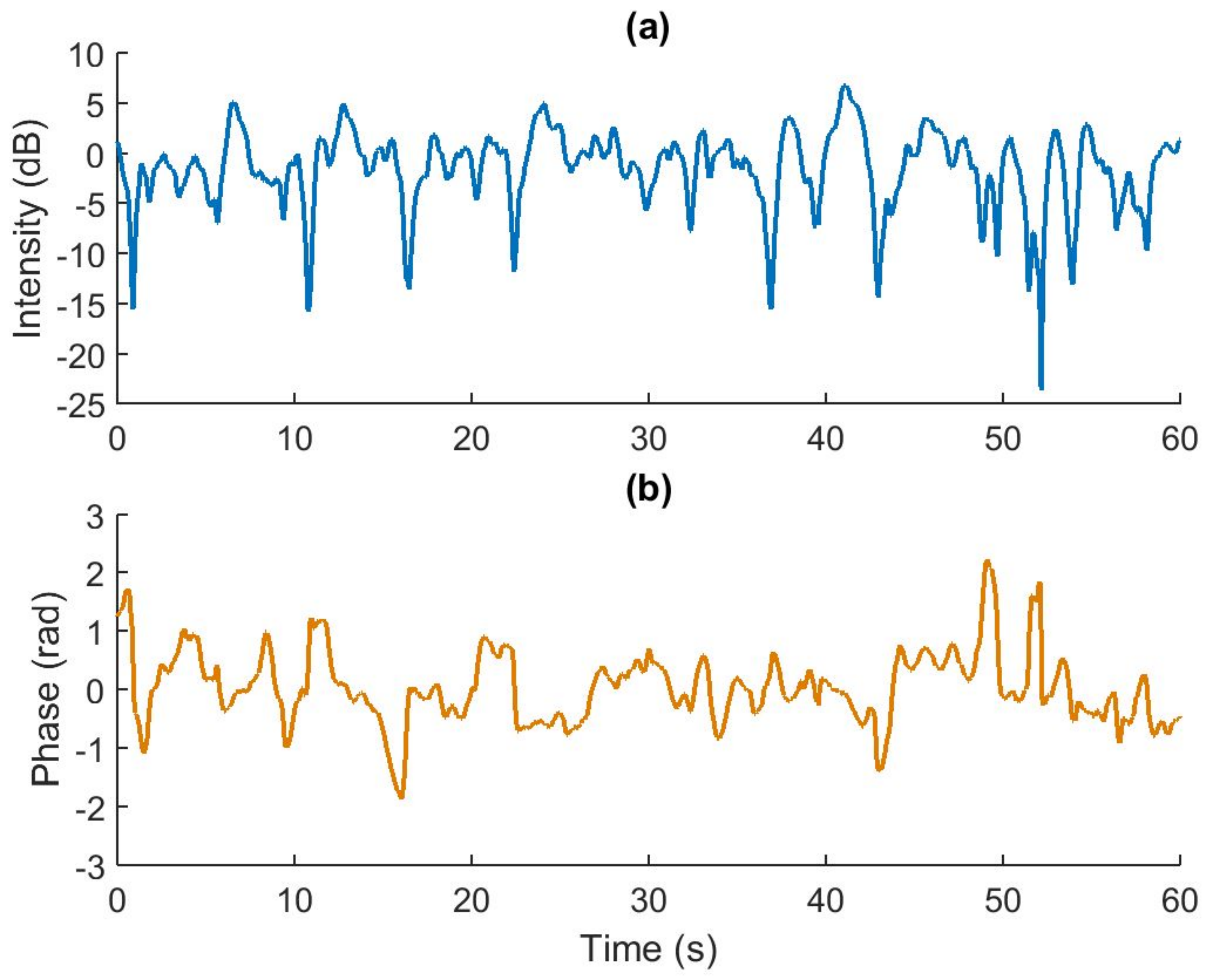

(a)
Intensity (dB)
10
5
0
-5
-10
-15
-20
-25
0
10
20
30
40
50
60
(b)
Phase (rad)
3
2
1
0
-1
-2
-3
0
10
20
30
40
50
60
Time (s)

Figure 4.

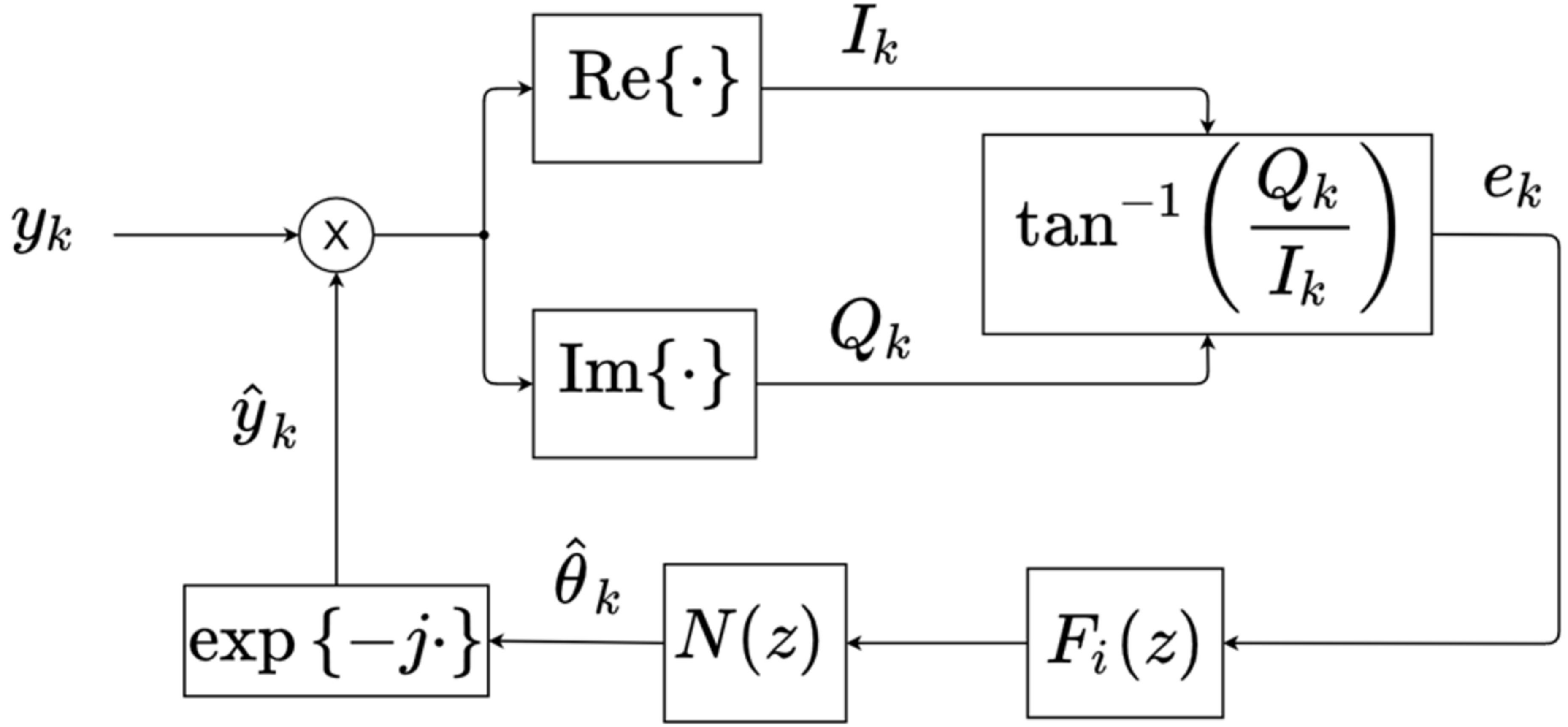
y_k
×
$\mathrm{Re}\{\cdot\}$
I_k
$\tan^{-1}\left(\frac{Q_k}{I_k}\right)$
e_k
$\mathrm{Im}\{\cdot\}$
Q_k
$\hat{y}_k$
$\hat{\theta}_k$
$\exp\{-j\cdot\}$
$N(z)$
$F_i(z)$

Figure 5.

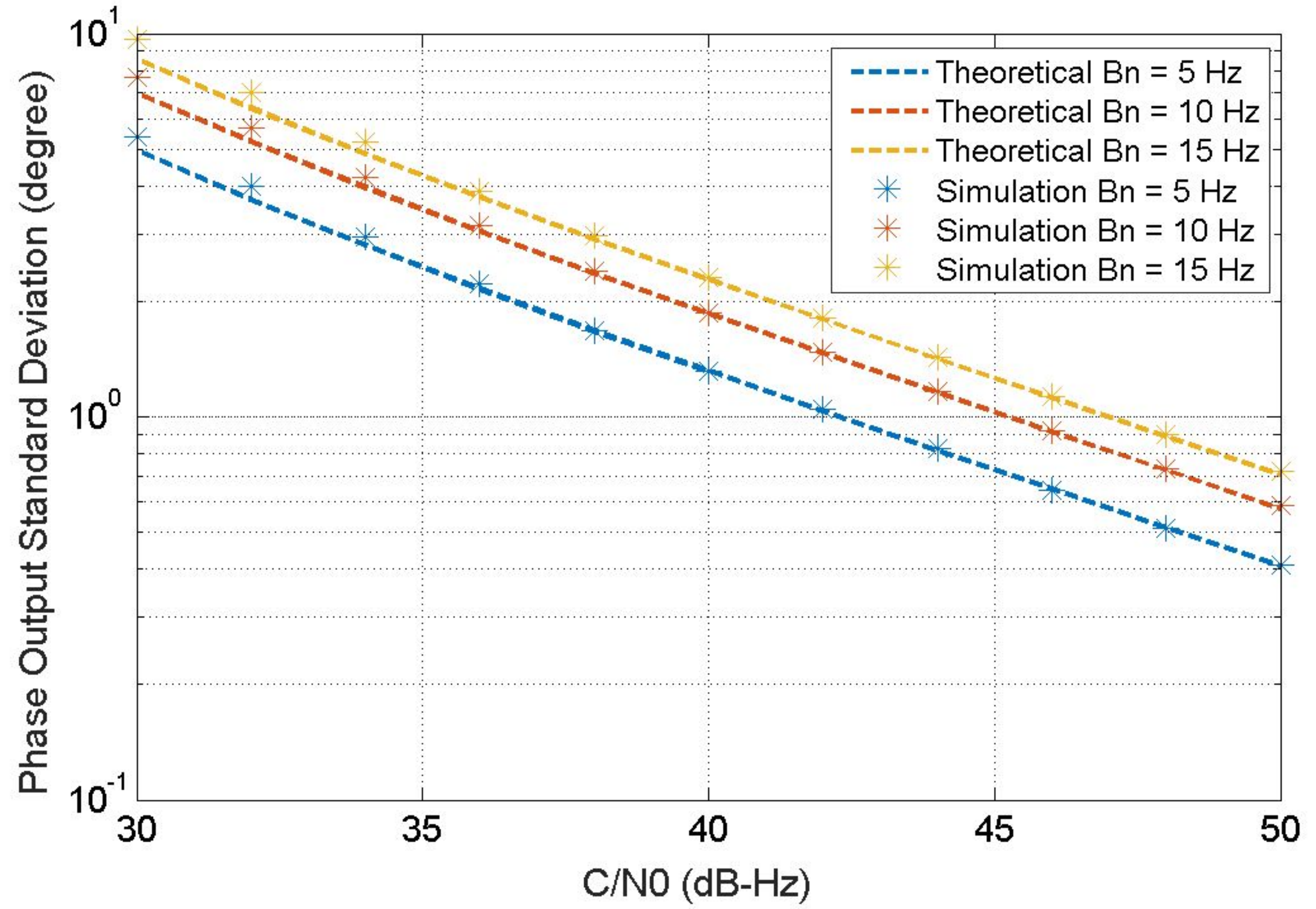

Theoretical Bn = 5 Hz
Theoretical Bn = 10 Hz
Theoretical Bn = 15 Hz
Simulation Bn = 5 Hz
Simulation Bn = 10 Hz
Simulation Bn = 15 Hz
Phase Output Standard Deviation (degree)
C/N0 (dB-Hz)
10^1
10^0
10^{-1}
30
35
40
45
50

Figure 6.

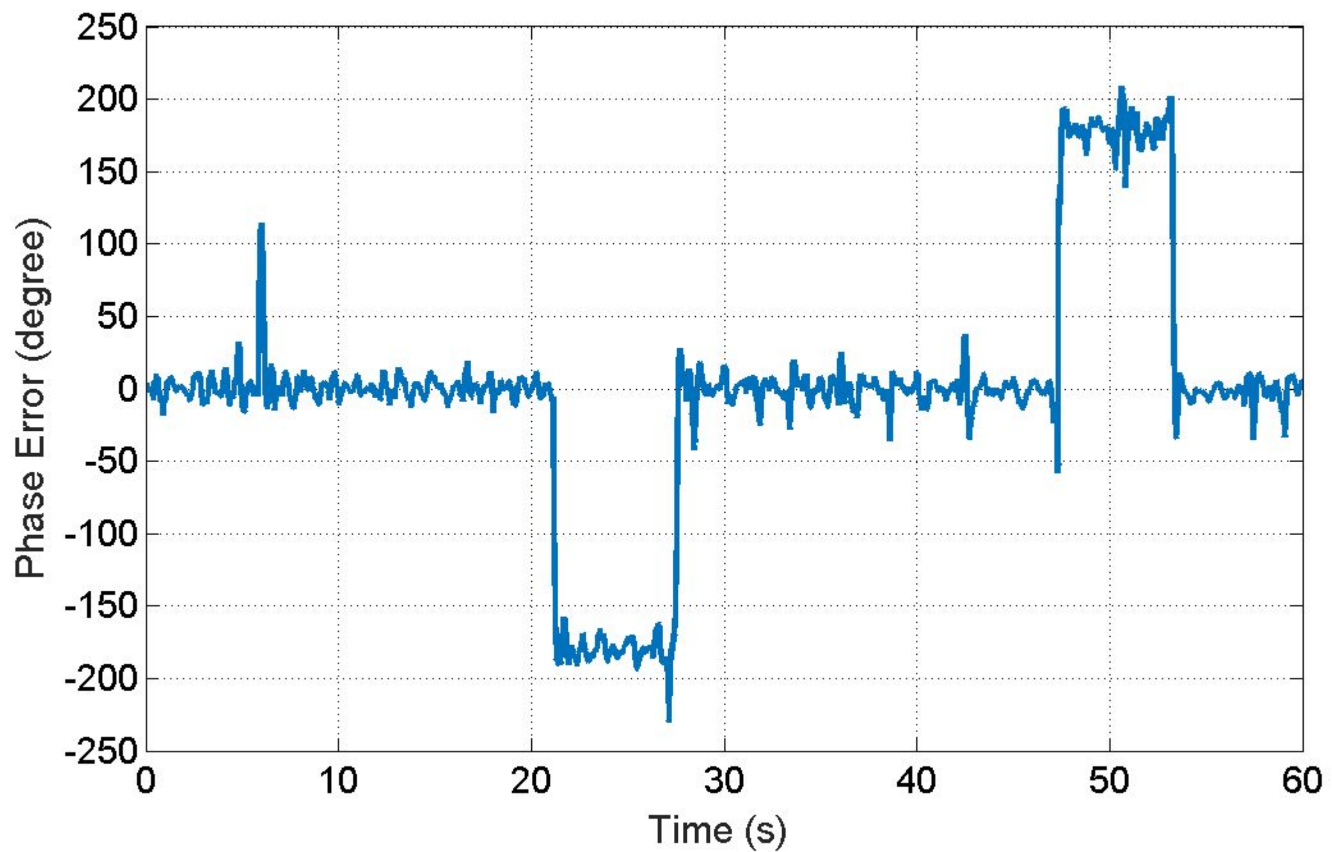
250
200
150
100
50
0
-50
-100
-150
-200
-250
Phase Error (degree)
0
10
20
30
40
50
60
Time (s)

Figure 7.

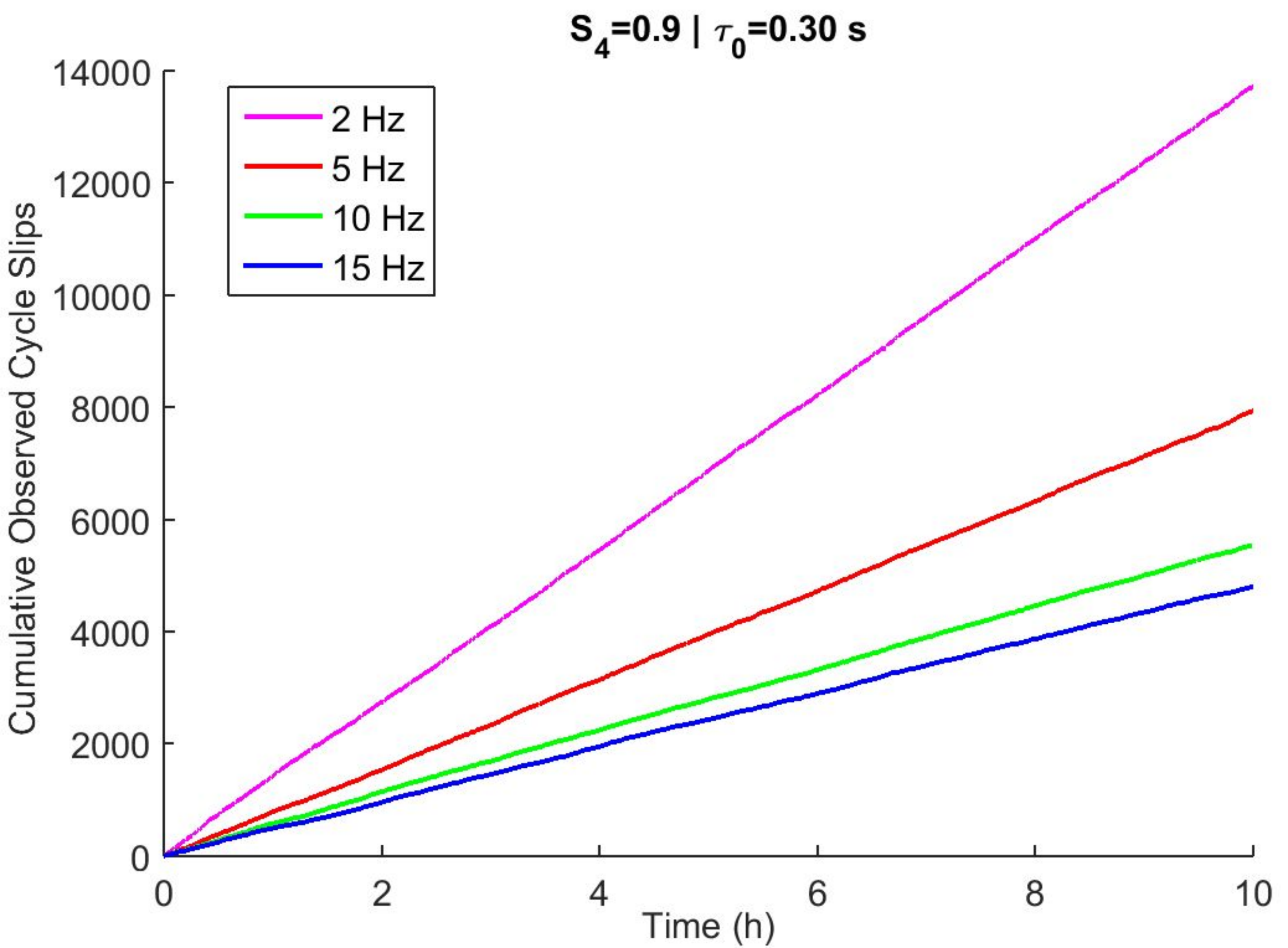
S4=0.9 | τ0=0.30 s
Cumulative Observed Cycle Slips
Time (h)
2 Hz
5 Hz
10 Hz
15 Hz
0
2000
4000
6000
8000
10000
12000
14000
0
2
4
6
8
10

Figure 8.

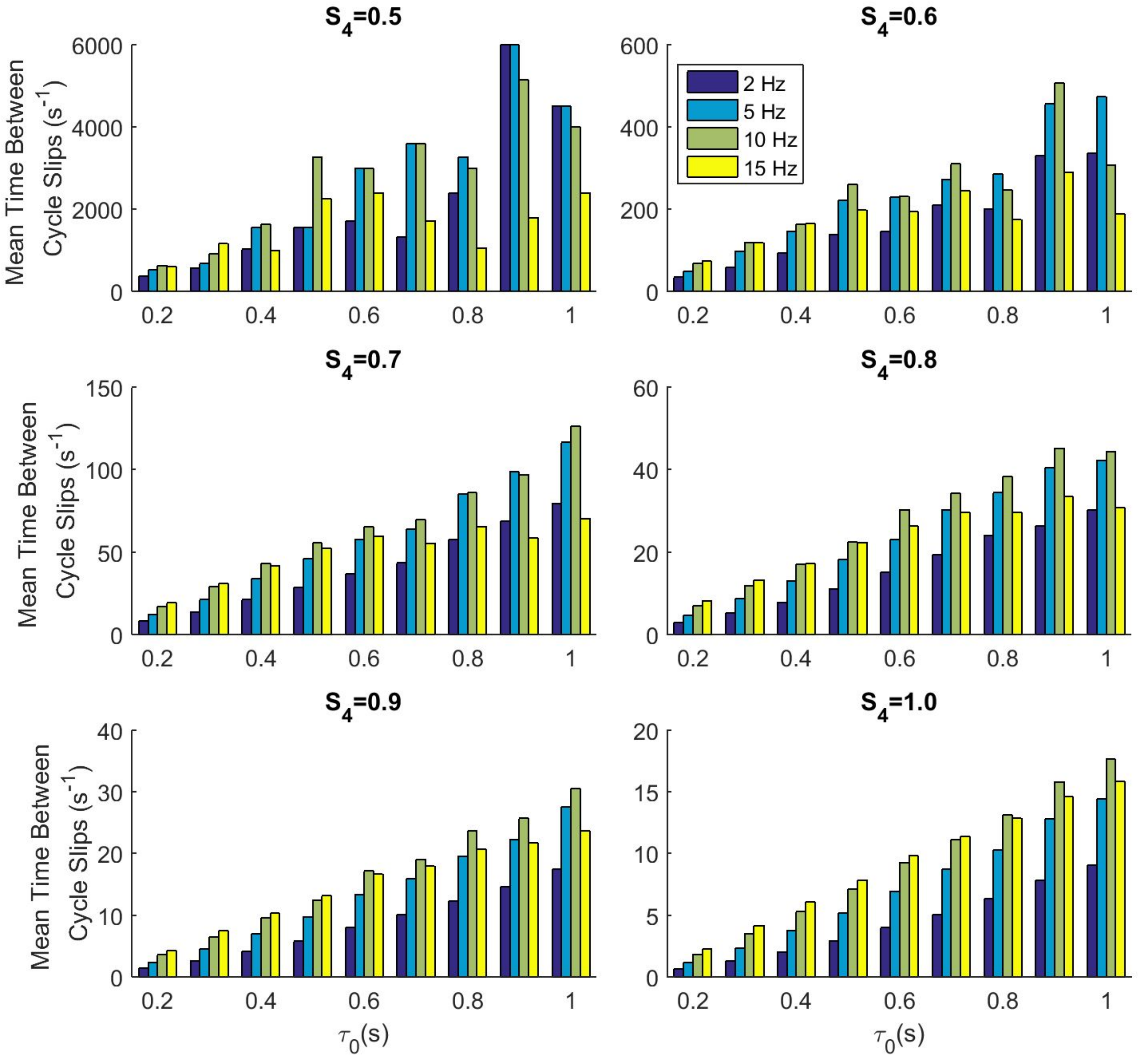
S4=0.5
S4=0.6
S4=0.7
S4=0.8
S4=0.9
S4=1.0
Mean Time Between Cycle Slips (s-1)
2 Hz
5 Hz
10 Hz
15 Hz
τ0(s)

Figure 9.

1.0
0.9
0.8
0.7
0.6
0.5
S4 level
0.2
0.3
0.4
0.5
0.6
0.7
0.8
0.9
1.0
τ0 (s)
15.0 15.0 15.0 15.0 15.0 15.0 10.0 10.0 10.0
15.0 15.0 15.0 15.0 10.0 10.0 10.0 10.0 10.0
15.0 15.0 15.0 10.0 10.0 10.0 10.0 10.0 10.0
15.0 15.0 10.0 10.0 10.0 10.0 10.0 5.0 10.0
15.0 15.0 15.0 10.0 10.0 10.0 5.0 10.0 5.0
10.0 15.0 10.0 10.0 10.0 10.0 5.0 5.0 5.0

Figure 10.

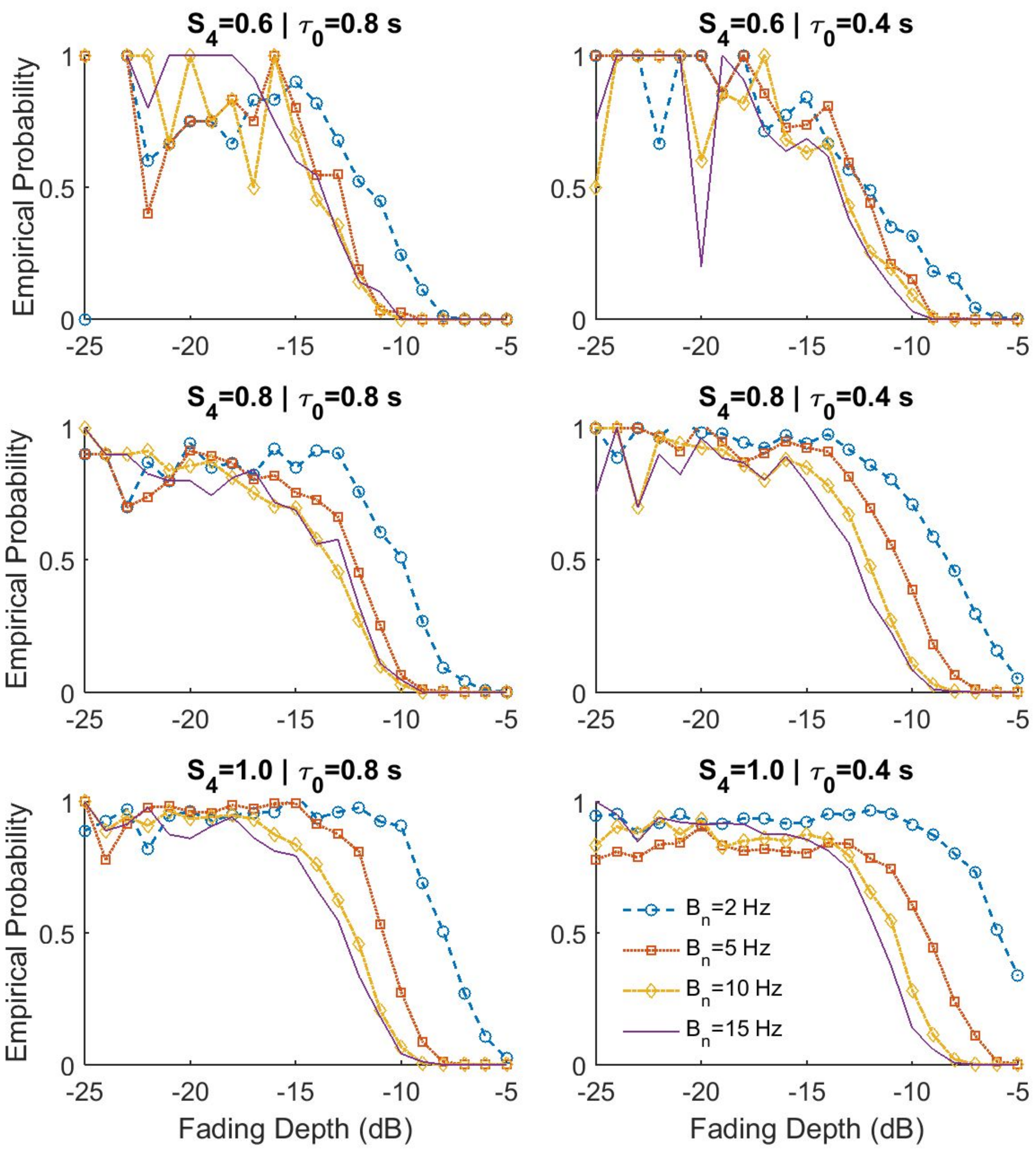

S4=0.6 | τ0=0.8 s
S4=0.6 | τ0=0.4 s
S4=0.8 | τ0=0.8 s
S4=0.8 | τ0=0.4 s
S4=1.0 | τ0=0.8 s
S4=1.0 | τ0=0.4 s
Empirical Probability
Fading Depth (dB)
Bn=2 Hz
Bn=5 Hz
Bn=10 Hz
Bn=15 Hz